Weak bond strength between successive layers in extrusion-based additive manufacturing : measurement and physical origin

Emmanuel Keita, Hela Bessaies Bey, Wenqiang Zuo, Patrick Belin, Nicolas Roussel

WEAK BOND STRENGTH BETWEEN SUCCESSIVE LAYERS IN EXTRUSION-BASED ADDITIVE MANUFACTURING: MEASUREMENT AND PHYSICAL ORIGIN

Emmanuel Keita, Hela Bessaies-Bey, Wenqiang Zuo, Patrick Belin, Nicolas Roussel*

* Corresponding author

Abstract:

Requirements on material properties for extrusion-based additive manufacturing mostly focus on the rheological behavior of the cementitious material being printed. The layer interface strength is therefore often considered to result from a proper mixing or remixing of two consecutive layers induced by the deposition process itself and therefore from the material thixotropic behavior. We show however here that, in the case of smooth interfaces, the drop in interface strength finds its origin in the water evaporation from the free surface occurring during the short time interval between two successive layers. Our results and their analysis within the framework of drying physics suggest that the water loss is localized in a dry region at the free surface leading to an incomplete cement hydration and high local porosity. We moreover compare here various experimental protocols allowing for the assessment of a drop in bond strength.

1. Introduction

Extrusion-based additive manufacturing is the dominant technology in the field of automated and digital manufacturing of concrete [1]. It consists in shaping the material by extruding it layer-by-layer through a mobile and digitally controlled nozzle. Such a technique imposes various rheological requirements on the printable material that are extremely different from the ones expected from a standard concrete shaped using a standard formative process [2].

The dominant and specific requirement deals with the ability of the material to turn, within an extremely short time-window, from a rather liquid pumpable suspension into a quasi-solid able to

carry its own weight without the help of a formwork or any support [3–5]. Minimum requirements for the structuration rate of the material have therefore recently been proposed [3,5,6] along with mix design strategies allowing for reaching such requirements.

Most of the above authors [3,5] also discussed the existence of a potential upper limit for this structuration rate. Such as discussion originates from the assessment of obvious weak interfaces or weak bonds between successive layers [3]. Such weak interfaces have been already studied in the case of standard fluid concretes [7]. They were described as so-called “cold joints” or as the consequences of a so-called “distinct-layers casting”.

Distinct layer casting was shown to find its origin in the absence of remixing at the interface between layers [7]. This feature was said to occur when the thixotropic nature of the material generates a fast increase in the consistency of the first layer, which, in turn, prevents the flow of second layer from re-initiating a flow of the first layer at the interface. Other authors [8] recently showed that distinct layer casting could also occur when the consistency of the material is too high to allow for a proper smooth contact between the two layers. Such a reduced effective contact area may therefore, in turn, reduce the bond strength.

In this paper, we first compare various experimental protocols allowing for the assessment of a drop in bond or interface strength. We then show that, in the case of smooth interfaces, the drop in interface strength finds its origin in the water evaporation from the free surface occurring during the short time interval between two successive layers. Our results and their analysis within the framework of drying physics suggest that the water loss is localized in a dry region at the free surface leading to an incomplete cement hydration and high local porosity.

2. Materials and protocols

2.1. Materials

A CEM I Cement (Saint Vigor, Lafarge) with a specific density of 3.15 iss used in this study. The Particle Size Distribution (PSD) was measured using a laser particle size analyzer (Malvern

Mastersizer S) by dispersion in isopropanol (Cf. Fig. 1). The median and maximum particle sizes are around 11.5 µm and 70 µm, respectively. Natural rounded sand with particle size ranging from 1 to 4 mm is used in this study. Its specific density is 2.6. Two commercial polycarboxylate-based High Range Water Reducing Admixture (HRWRA), Sika Viscocrete Tempo 12 and Sika Viscocrete Krono 947, were used in this study. Specific density and solid concentration of Tempo 12 are 1.060 ± 0.020 and 29.5% ± 1.4%, respectively. Specific density and solid concentration of Krono 947 are 1.060 ± 0.010 and 32.5% ± 1.6%, respectively.

Five different flowable mortars with water to cement ration (W/C) ranging from 0.20 to 0.45 are studied in this paper. Their mix proportions and yield stresses are shown in Table 1. It should be noted that the yield stresses of these mortars were initially assessed from slump test measurement and analysis according to [9]. Mix design was then adjusted for yield stress to stay in the range of 15 Pa to 35 Pa in order to limit fresh surface roughness after casting of the first layer under the sole effect of gravity and to ensure a full and smooth contact between layers [8].

2.2. Mixing and samples preparation

For all mortars, a volume of 1.8 L was mixed using a planetary mixer at a constant speed of 67 rpm. The HRWRA was added to water before contact with cement.

For mortars with W/C ranging from 0.45 **down to 0.25**, water and cement were first mixed for 30 s to obtain a homogenous cement paste. Sand was then added into the mixing bowl within 30 s and mixed for another 90 s. After that, the mixer was stopped and walls of the mixing bowl were scrapped within 30 s. Finally, the mixtures were mixed for another 60 s. The mixing process total duration was 4 min.

For the mortar with W/C 0.20, a longer mixing process was needed due to the difficulty of mixing such a high amount of solid materials with the corresponding low water content. Water and cement were therefore first mixed for 120 s to obtain a homogenous cement paste. Then, the sand was

slowly added to the paste within 240 s. After sand addition, the resulting mixture was mixed for another 480 s. The mixing process total duration was 12 min.

A first layer of all mixtures with a thickness of 20 mm was cast into a rigid triple rubber mold with dimensions 40 mm × 40 mm × 160 mm in the 5 minutes following the end of mixing. As the initial yield stress is low (see Fig. 3), the mortar is self leveling and the surface of the first layer is smooth. These first layers were then placed in a wind tunnel (see section 2.4). Some molds containing these first layers were also sealed with a plastic film and stored to prevent any water evaporation. After a given resting time ranging from 10 minutes to 24 hours, a second 20 mm layer of material was cast above the first one by slowly flowing the liquid mortar. No vibration or external mechanical energy was brought to any of the samples during casting of any of the layers.

For all samples with resting times between layers less than 30 min, the same batch was used. Before the casting of the second layer, the mixtures were stirred manually in order to prevent any major workability loss. For all samples with resting times between layers higher than 30 min, a new batch was prepared.

2.3. Rheological measurements

The rheological measurements were carried out using a C-VOR Bohlin stress-controlled rheometer equipped with Vane geometry. The Vane geometry was a four-bladed paddle with a diameter of 25 mm, the outer cup diameter was 50mm and its depth was 60 mm. Each sample was poured into the rheometer cup just after mixing and left at rest for either 10, 30, 60 or 120 minutes. A new sample was prepared for each of these resting times. After the chosen resting time, the measurement sequence started by simply applying a constant shear rate of 0.1 s^{-1}, at such low shear rate, viscous contribution to the shear stress is negligible compare to the yield stress. The peak of the measured shear stress curve at flow onset or the so-called “static yield stress” was extracted from the shear stress measurement [10].

2.4. Mechanical testing

Adhesion is a delicate property to measure and there exist various mechanical tests in literature [11]. We chose here to avoid any tests requiring any cutting or sawing. We moreover avoided any gluing between the samples and the mechanical press components. We therefore chose to perform on our samples the flexion and compression tests shown in Fig. 2.

The mechanical answer of all samples was assessed 7 days after the casting of the first layer. We used a combined compression and flexural testing machine (CONTROLS PILOT4 C300kN). The samples were first broken into two parts through the three-points bending test (See Fig. 2 left).

Then we performed the three different compression tests shown in Fig. 2. The first test method was the traditional compression test of the samples with a bearing area of 40 mm × 40 mm according to ASTM C109. The latter two test methods were carried with the help of either iron blades or iron angles with a thickness of 1 mm and a contact area with the sample of 10 mm × 80 mm and 25 mm × 45 mm, respectively. For all tests, the loading rate was kept constant and equal to 2400 N/s and the peak force needed to fracture the sample was recorded.

2.5. Wind tunnel

The wind tunnel used here has a cross section 50 X 70 cm and is crossed by a dry air flux at 80 L/min corresponding to an average air velocity of $3.8 \cdot 10^{-3}$ m/s [12]. The dew point of the air is -40°C, corresponding to a RH lower than 1%. The general drying rate is slightly increased compared to room conditions but it is constant during an experiment and over the seasons. The evaporated water mass in the first layer is continuously measured while the sample is in the wind tunnel and before the casting of the second 20 mm layer.

2.6. SEM analysis

The mortar samples were impregnated with epoxy resin (Epofix from Struers). They were then polished using Silicon carbide abrasive papers, diamond spray and ethanol as lubricant. The polished sections were then coated with a thin carbon deposit. The microstructure of the interface between layers was then investigated by backscattered electrons mode on a FEI Quanta 400 Scanning Electron Microscope (SEM).

3. Experimental results

3.1. Rheological measurements

We plot in Fig. 3 the relative yield stress (*i.e.* the ratio between the yield stress after a given period of rest and the initial yield stress) as a function of resting time. It can be noted that, in the case of the mixture with a W/C ratio of 0.2, measurements could not be carried after 60 minutes of rest as the required torque exceeded the capacity of the rheometer. The average structuration rates of the materials are 12 Pa/min for W/C = 0.4, 15 Pa/min for W/C = 0.35 and 27 Pa/min for W/C = 0.2. Despite their initial high fluidity, these mixtures are all highly thixotropic according to the classification proposed in [13].

3.2. Mechanical testing

We prepared samples for mechanical testing following the procedure described in section 2.2 and 2.4. The number of samples per configuration is shown in Tab. 2. Such a high number of samples was needed in order to assess the standard deviations of the various tests and their sensitivity to the presence of a weak interface in the sample.

The reference sample was monolithic and cast in one layer of 4 cm whereas the so-called “layered sample” was prepared with the W/C = 0.35 mortar. The second layer of the layered sample was cast after a 2 hours rest of the first layer in the wind tunnel described in section 2.5.

We plot in Fig. 4 the relative bond strength (*i.e.* the ratio between the average strength measured for the layered sample and the average strength measured for the reference sample) for the various tests configurations.

We first note that, for all tests, when there is an interface in the sample, standard deviation increases. This is expected as, no matter the physical origin of the weak interface, we introduce a variable local weakness in the system. The mechanical answer deviates from the one of an homogeneous material and starts to be affected by the weakness level of the interface and its details.

We moreover note that, apart from the increase in standard deviation, both bending and compression tests are not able to detect the presence of the interface. This was expected as both flexion and compression because of their specific stress path do not test the interface directly. The resulting average measurement is therefore only weakly affected by the presence of a weak interface.

Both blades and angles test allow for the measurement of a drop in the average relative strength. However, the blade configuration tests only the interface and, as such, provides a very scattered measurement. The angle test appears to be an intermediate mechanical loading predominantly shearing the material, as the fracture path has to cross the interface and can therefore only use the interface as the weakest path or go through both the bulk and the interface.

From the above experimental results, it can therefore be suggested that, among the tests compared here, only the angles test allows for the measurement of a drop in average relative bond strength larger than the test standard deviation. This test will therefore be used for the rest of this paper.

3.3. Relative bond strength as a function of resting time

We plot in Fig. 5 the relative bond strength as a function of resting time for our 0.2 W/C ratio mortars cast in two layers. We see that, when the first layer is protected from drying, interface strength remains constant with increasing resting time between layers up to 2 hours. We then

observe a slight decrease after 5 hours (*i.e.* when resting time is of the order of or higher than setting time).

On the contrary, relative bond strength decreases for resting times as short as 10 minutes when the first layer is submitted to drying. Relative interface strength decreases then constantly during the first hour of rest and reaches a plateau afterwards at half its initial value.

The constant relative strength for sealed layers of this highly thixotropic material suggests that, contrarily to literature [7], the decrease in bond strength is not related to thixotropy and structuration of the first layer. It suggests that it finds its origin in the drying of the resting first layer.

3.4. Water loss as a function of resting time

We plot in Fig. 6 the relative water loss in the first layer *(i.e*. the ratio between the mass of evaporated water and the initial mass of water in the sample) as a function of the resting time before the casting of the second layer.

We see that water loss in the sealed samples, being lower than 0.1 % of the initial water mass in the sample, is neglectable. We moreover note that the controlled drying in the wind tunnel allows for a final water loss around 2 times higher than room drying. Finally, it is worth noting that the water loss for the samples that stayed in the wind tunnel stays rather low too, being of the order of a couple %. If we consider that this water loss is homogeneous, such a low drop in available water should not affect cement hydration and therefore be at the origin of decrease in mechanical strength. This suggests that this water loss is localized athe free surface of the first layer.

4. Analysis

We recall here that the initial drying rate in the resting first layer is expected to be roughly the same for all experiments and to be driven by the drying conditions imposed by the wind tunnel. It should however be kept in mind that this drying rate could be affected by the sample temperature and

therefore by the W/C ratio of the system (see discussion section). From the measured drying rate in Fig. 6, we can compute the flow of liquid water at the free surface for a given experiment:

$$J_e = \frac{-1}{\rho_0 S}\frac{\mathrm{d}m}{\mathrm{d}t} \quad (1)$$

Where S = 6.4 x10^{-3} m^2 is the surface area and ρ_0 = 1000 kg/m^3 is the water density. In this study, the initial drying flux at the free surface is therefore around 10^{-7} m/s for all experiments.

Previous studies on drying of porous media have shown that, regardless of the nature of the porous material structure, evaporation at the free surface is at the origin of a capillary pressure gradient [14–17]. Two drying regimes were then identified in literature:

- In a first regime, the water flow induced by the capillary gradient balances the evaporation rate. The limit between the wet and the dry region stays at the free surface and does not move towards the interior of the porous medium. The water loss is then distributed homogeneously in the sample leading, in the case of a rigid porous medium, to an overall decrease in the liquid saturation level.
- In a second regime, the water flow induced by the capillary gradient is not able to balance the evaporation rate. The liquid does not have time to flow and replace the evaporated liquid. A dry region is then expected to develop from the free surface and to propagate in the sample. Water loss can then be extremely localized at the free surface.

The transition between these two regimes depends on the capacity of the porous medium to provide water to the free surface [14–16]. We assume here that water flows in the porous medium according to Darcy's law with a pressure gradient dominated by the capillary pressure as, in our experiments, gravitation effects can be neglected. Thus, the maximal capillary flow writes [15,16,18–20]:

$$J_{cap} = \frac{\phi}{\eta H} k \cdot P_{cap} \quad (2)$$

Where η is the liquid viscosity, H the sample height, k the permeability, ϕ the porosity and P_{cap} the capillary pressure. We estimate here the maximal capillary flow J_{cap} for our different systems. The water (or interstitial fluid) viscosity is $\eta = 1\,\text{mPa.s}$. The capillary pressure is of the order of γ/r where $\gamma = 70\,\text{mN/m}$ is the air/water surface tension and r is the pore size. For the sake of simplicity, we consider here $r = 1\,\mu\text{m}$, as being independent from mix design. ϕ depends on water-to-cement ratio and sand volume fraction. We estimate the permeability of the mortars by using the Kozeny-Carman formula $k = \phi^3 r^2 / 45(1-\phi)^2$. We obtain permeability values for our fresh materials ranging between 10^{-15} and 10^{-16} m^2 in good agreement with experimental measurements from [21].

Using Eq. (2), we then estimate that the maximal capillary flow for our mortar at W/C = 0.45 containing 45% volume sand is around 10^{-6} m/s while it decreases down to 10^{-7} m/s for our mortar at W/C = 0.20 containing 50% volume sand.

We can therefore conclude that, for our higher water-to-cement ratio mortars, $J_{cap} \approx 10 J_e$ and drying is in the first regime described above. The material shall be able to provide water to the free surface and water loss is therefore expected to be homogeneously distributed in the sample. On the other hand, for our lowest water-to-cement ratio mortars, the maximal capillary flow becomes close to the evaporative flux, $J_{cap} \approx J_e$. Literature [20] has shown that, as soon as the evaporative flux is of the same order of magnitude as the maximal capillary flow, the porous material becomes unable to provide water to the free surface. A dry front is then expected to penetrate the material and water loss shall be localized close to the drying interface.

Such a dry front can be visualized using SEM experiments on our hardened samples. We show in Fig. 7 three representative pictures of the layers interface in three extreme cases. On the right figure, we show the interface for W/C ratio = 0.2 after 10 minutes resting time for a sealed sample (*i.e.* no drying of the first layer). We see that, apart from a local particle wall effect at what was the free surface of the first layer, there is no visible interface. On the center picture, we show the interface

for W/C ratio = 0.35 after 120 minutes resting time in the wind tunnel. A more porous zone of a thickness of around 100 micrometers is detected. If this higher porosity was induced by flow or processing, it would be visible in some of our sealed samples, which was never the case. We suggest therefore here that this higher porosity zone finds its origin into a localized local water loss induced by drying and it consequences on the degree of hydration of the cement. Finally, we show in the right picture the interface for W/C ratio = 0.35 after 24 hours drying time in the wind tunnel. The same higher porosity layer is present with a thickness of around 500 micrometers.

We now plot in Fig. 8 the measured relative interface strength as function of the W/C ratio for a 120 minutes resting time. We note that, above a W/C ratio of 0.45, the interface strength seems to tend towards the reference value for a monolithic sample. Below a water-to-cement ratio of 0.35, the interface strength reaches a minimum plateau value.

We suggest that, as long as the material is able to feed the surface with water during drying, there are no consequences of resting on relative interface strength. However, for W/C ratios lower than 0.45, the water recedes in the sample leaving behind a zone where there is not enough water to fully hydrate the cement powder. Although this zone has a thickness of the order of a couple hundreds micrometer, we suggest it is sufficient to induce a mechanical weakness of the layers interface.

5. Discussion

The results shown here suggest that, in the worst case studied here (*i.e.* W/C ratio of 0.2 and 50% volume sand), a critical ten minutes resting time was sufficient to induce a drop in interface strength (Cf. Fig. 5). Such a resting time is still compatible with most common extrusion-based additive manufacturing processes [1,5]. This critical resting time increased when the W/C ratio increases up to W/C = 0.4 as shown in Fig. 8. Finally, for W/C ratio above a critical value of 0.4, no decrease in interface strength was measured. This means that most materials that are being printed today could, at first, seem to be unaffected by the features presented here. We discuss below why it shall not be the case in practice.

5.1. Effect of material temperature

We have considered in this paper non-accelerated materials (*i.e.* hydration occurred at a natural rate). Printable concretes are often accelerated in order to enhance the ability of the material to build up a structure allowing for the material to be printed without any supports. Most acceleration technologies used in practice are based on either enhancing the aluminates reaction or enhancing the silicates hydration [22]. Both strategies lead to a strong increase of the heat release at very early ages and an increase of the material temperature [4]. In the case of the printing systems where no acceleration is used, the printable material often displays extremely stiff consistency. This consistency is needed for the material to withstand its self-weight through the printing process. Its pumping and its extrusion generate high level of friction and, here again, temperature increases.

Taking as a reference a sample at 20°C in a 50% HR environment, an increase of 5°C of the material temperature is expected to increase the drying rate by 15% while an increase of 10°C is expected to increase it by 80%. As the drying rate increases, the material switches to the second drying regime, in which water loss is localized at the surface for lower W/C ratio or shorter resting times. This localized water loss is then able to prevent cement hydration and induces a decrease in interface strength.

5.2. Effect of mix proportions

Low W/C ratio and high amount of aggregates shall both lead to a decrease in porosity and therefore a decrease in permeability. This, in turn, shall decrease the ability of the material to feed the surface with water under the effect of a capillary pressure gradient induced by drying. Non-adsorbed polymers/admixtures shall moreover increase the viscosity of the interstitial liquid [23] decreasing also its ability to flow towards the surface and balance the water loss [24]. Both features have the same effect. They push the material into the second drying regime, in which water loss is localized at the surface for lower critical W/C ratio or shorter critical resting times

5.3. Effect of the environment

First, it has to be kept in mind that the only reason we used a wind tunnel in this study was because we wanted to impose a well-controlled and constant drying rate. The average air velocity is low but insure a replacement of the tunnel air. The overall drying imposed to the samples was of the same order as the average one imposed by storing the samples in the lab, Cf. Fig. 6.

As drying was shown here to play a dominating role on the formation of weak interfaces, this suggests that the environmental conditions for the printing process (temperature and relative humidity) are of the most utter importance. It can then be expected that printing outside shall be more delicate than printing within the controlled environment of a laboratory or even within a precast factory.

5.4. Effect of thixotropy and remixing

We have shown here that thixotropy is not the dominating limiting factor for interface strength in the case of extrusion-based additive manufacturing processes. The presence of a dried zone in the first layer shows that the second layer is not able to remix the first layer for the casting process studied here. This was to be expected, as the shear induced by the simple deposition of a layer of centimetric thickness is too weak to initiate or reinitiate flow. This means that using the cold joint prediction model developed in [7] shall not bring any insights for requirements on resting time between layers. It is however interesting to note that, as the weak dried zone thickness is around several hundreds of micrometer, a local “mechanical” remixing could allow for a re-homogenization of the local water content and delete the consequences of drying on the upcoming hydration reaction. This feature cannot come from the casting of the second layer itself but could be generated by the printing head. Vaporization of water after deposition of the first layer could also compensate for the water loss and could be a promising and practically doable solution.

6. CONCLUSIONS

We have tested various experimental protocols allowing for the assessment of a drop in bond strength between successive layers in additive manufacturing. These protocols did not require any sawing or polishing of the samples after casting. From the measured amplitude variations and the measurement standard deviations, we suggested that an adequate protocol could lie in the use of metal corners or angles allowing for a concentration of stress in the area containing the interface.

Some mechanical testing did not show any significant deviation in the presence of a weak interface. As a consequence, care should be taken before concluding that a given printable concrete along with a given deposition process are fine from an interface strength point of view.

We have shown that, for flowable mortars with low water to cement mass ratio, a drop in interface strength does not find its origin in the structural build up of the bottom layer that could prevent the remixing of two successive layers. Our results however suggested that a superficial extremely localized drying is at the origin of a drop in bond strength.

We moreover suggested that this localization finds its origin in the fact that, for low porosity fresh materials, the liquid does not have time to flow and replace the evaporated liquid. As a consequence, a dry region is then expected to develop from the drying interface and to propagate in the sample. In this region, there is not enough water to hydrate the cement powder and the interface strength decreases.

ACKNOWLEDGEMENT

This work has been carried out within the frame of the project DiXite. Initiated in 2018, DiXite is part of I-SITE FUTURE, a French initiative to answer the challenges of sustainable city. We acknowledge the help of Beatrice Desrues (IFSTTAR) for the SEM measurements.

REFERENCES

[1] R.A. Buswell, W.R. Leal de Silva, S.Z. Jones, J. Dirrenberger, 3D printing using concrete

extrusion: A roadmap for research, Cem. Concr. Res. 112 (2018) 37–49. doi:10.1016/j.cemconres.2018.05.006.

[2] N. Roussel, Rheology of fresh concrete: From measurements to predictions of casting processes, Mater. Struct. Constr. 40 (2007) 1001–1012. doi:10.1617/s11527-007-9313-2.

[3] T. Wangler, E. Lloret, L. Reiter, N. Hack, F. Gramazio, M. Kohler, M. Bernhard, B. Dillenburger, J. Buchli, N. Roussel, R. Flatt, Digital Concrete: Opportunities and Challenges, RILEM Tech. Lett. 1 (2016) 67. doi:10.21809/rilemtechlett.2016.16.

[4] L. Reiter, T. Wangler, N. Roussel, R.J. Flatt, The role of early age structural build-up in digital fabrication with concrete, Cem. Concr. Res. 112 (2018) 86–95. doi:10.1016/j.cemconres.2018.05.011.

[5] N. Roussel, Rheological requirements for printable concretes, Cem. Concr. Res. 112 (2018) 76–85. doi:10.1016/j.cemconres.2018.04.005.

[6] A. Perrot, D. Rangeard, A. Pierre, Structural built-up of cement-based materials used for 3D-printing extrusion techniques, Mater. Struct. Constr. 49 (2016) 1213–1220. doi:10.1617/s11527-015-0571-0.

[7] N. Roussel, F. Cussigh, Distinct-layer casting of SCC: The mechanical consequences of thixotropy, Cem. Concr. Res. 38 (2008) 624–632. doi:10.1016/j.cemconres.2007.09.023.

[8] V.N. Nerella, S. Hempel, V. Mechtcherine, Effects of layer-interface properties on mechanical performance of concrete elements produced by extrusion-based 3D-printing, Constr. Build. Mater. 205 (2019) 586–601. doi:10.1016/j.conbuildmat.2019.01.235.

[9] N. Roussel, P. Coussot, “Fifty-cent rheometer” for yield stress measurements: From slump to spreading flow, J. Rheol. (N. Y. N. Y). 49 (2005) 705–718. doi:10.1122/1.1879041.

[10] N. Roussel, G. Ovarlez, S. Garrault, C. Brumaud, The origins of thixotropy of fresh cement pastes, Cem. Concr. Res. 42 (2012) 148–157. doi:10.1016/j.cemconres.2011.09.004.

[11] J. Silfwerbrand, H. Beushausen, L. Courard, Bond, in: B. Bissonnette, L. Courard, D. Fowler, J. Granju (Eds.), Bond. Cem. Mater. Overlays Repair, Lining or Strength. Slabs or Pavements,

RILEM State of the Art Reports, 2011.

[12] J. Naël-Redolfi, E. Keita, N. Roussel, Water absorption measurement of fine porous aggregates using an evaporative method: Experimental results and physical analysis, Cem. Concr. Res. 104 (2017) 61–67. doi:10.1016/j.cemconres.2017.11.003.

[13] N. Roussel, A thixotropy model for fresh fluid concretes: Theory, validation and applications, Cem. Concr. Res. 36 (2006) 1797–1806. doi:10.1016/j.cemconres.2006.05.025.

[14] F. Chauvet, P. Duru, S. Geoffroy, M. Prat, Three Periods of Drying of a Single Square Capillary Tube, Phys. Rev. Lett. 103 (2009) 1–4. doi:10.1103/PhysRevLett.103.124502.

[15] P. Coussot, Scaling approach of the convective drying of a porous medium, Eur. Phys. J. B-Condensed Matter Complex Syst. 15 (2000) 557–566. **doi:10.1007/s100510051160.**

[16] A.G. Yiotis, D. Salin, E.S. Tajer, Y.C. Yortsos, Drying in porous media with gravity-stabilized fronts: Experimental results, Phys. Rev. E - Stat. Nonlinear, Soft Matter Phys. 86 (2012) 026310. doi:10.1103/PhysRevE.86.026310.

[17] N. Shokri, D. Or, What determines drying rates at the onset of diffusion controlled stage-2 evaporation from porous media?, Water Resour. Res. 47 (2011) 1–8. doi:10.1029/2010WR010284.

[18] B. Camassel, N. Sghaier, M. Prat, S. Ben Nasrallah, Evaporation in a capillary tube of square cross-section: application to ion transport, Chem. Eng. Sci. 60 (2005) 815–826. doi:10.1016/j.ces.2004.09.044.

[19] E. Keita, P. Faure, S. Rodts, P. Coussot, MRI evidence for a receding-front effect in drying porous media, Phys. Rev. E. 87 (2013) 062303. doi:10.1103/PhysRevE.87.062303.

[20] E. Keita, T.E. Kodger, P. Faure, S. Rodts, D.A. Weitz, P. Coussot, Water retention against drying with soft-particle suspensions in porous media, Phys. Rev. E. 94 (2016) 033104. doi:10.1103/PhysRevE.94.033104.

[21] V. Picandet, D. Rangeard, A. Perrot, T. Lecompte, Permeability measurement of fresh cement paste, Cem. Concr. Res. 41 (2011) 330–338. doi:10.1016/j.cemconres.2010.11.019.

[22] D. Marchon, S. Kawashima, H. Bessaies-Bey, S. Mantellato, S. Ng, Hydration and rheology control of concrete for digital fabrication: Potential admixtures and cement chemistry, Cem. Concr. Res. 112 (2018) 96–110. doi:10.1016/j.cemconres.2018.05.014.

[23] J. Hot, H. Bessaies-Bey, C. Brumaud, M. Duc, C. Castella, N. Roussel, Adsorbing polymers and viscosity of cement pastes, Cem. Concr. Res. 63 (2014) 12–19. doi:10.1016/j.cemconres.2014.04.005.

[24] E. Keita, Y. Rifaai, P. Belin, N. Roussel, Influence of non-adsorbing polymers on drying of fresh mortars, Cem. Concr. Res. (2018). doi:10.1016/j.cemconres.2018.10.016.

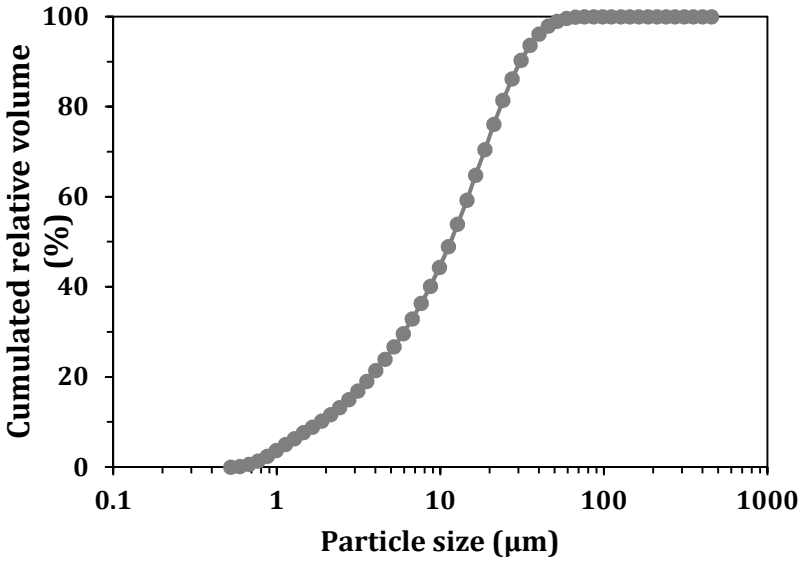

Figure 1: Particle size distribution of the cement used in this study.

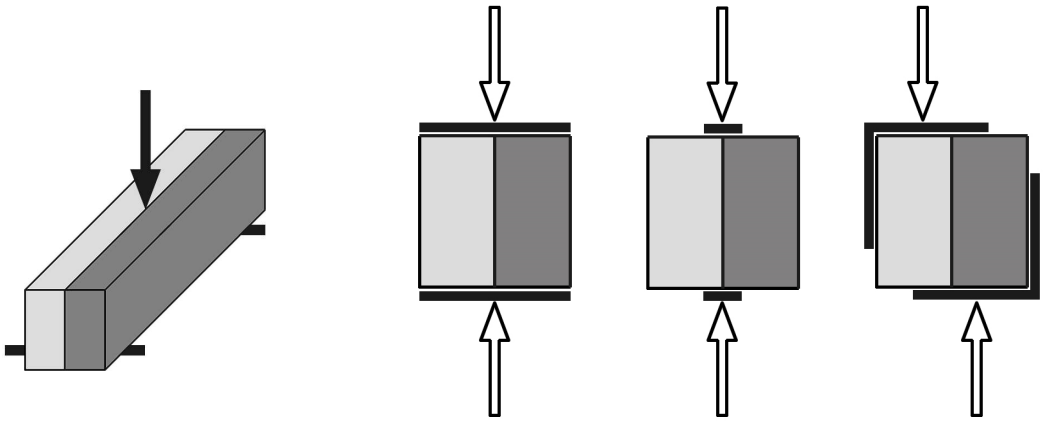

(a) *(b)* *(c)* *(d)*

Figure 2: The four mechanical testing configurations studied in this paper.(a) three points bending test. (b) Compression test (c) Compression test with iron blades at the interface of the two layers. (d) Compression test with iron angles.

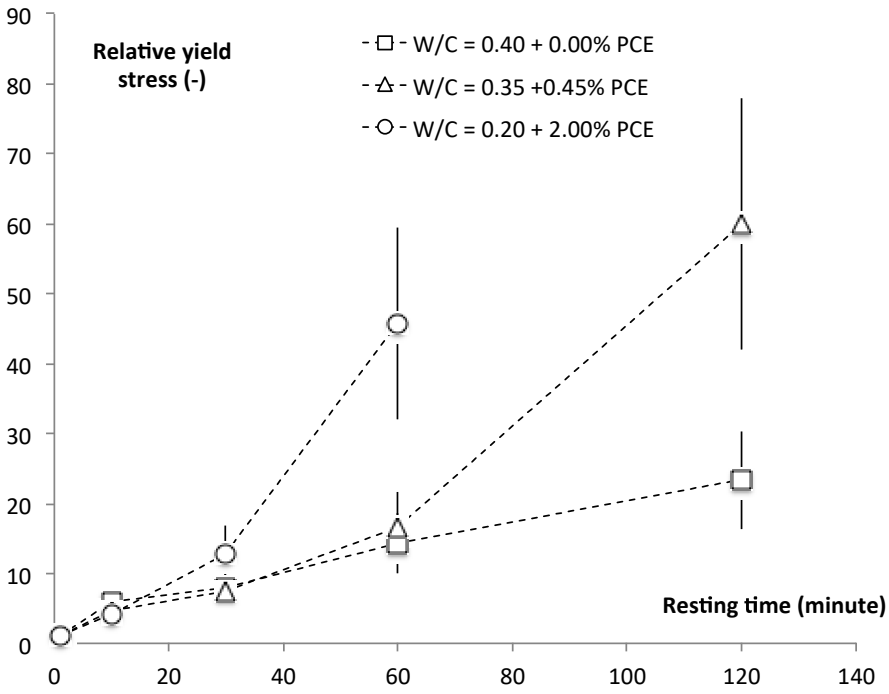

Figure 3. Relative yield stress (i.e. the ratio between the yield stress after a given period of rest and the initial yield stress) as a function of resting time for three of the mortars studied in this work.

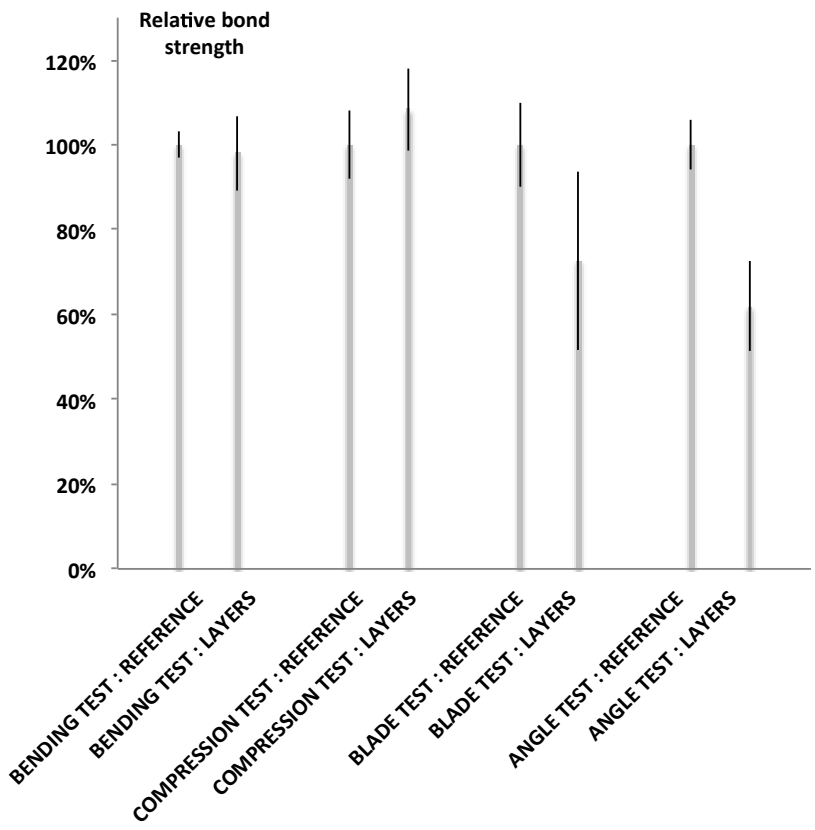

Figure 4. Relative bond strength as measured by the four different tests. Average and standard deviation are plotted.

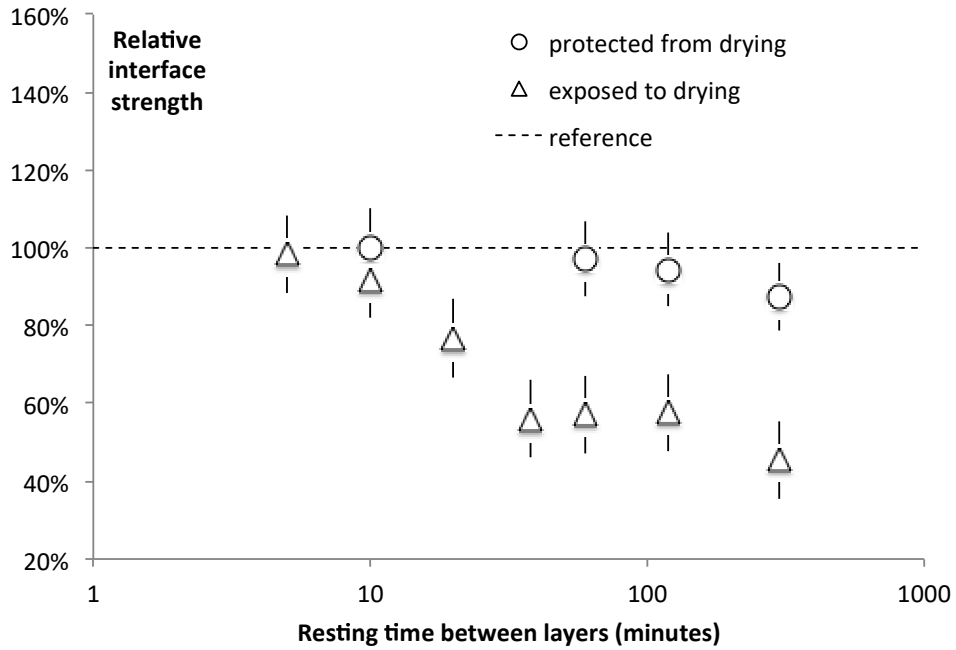

Figure 5. Relative interface strength as a function of resting time for a sealed first layer and a first layer exposed to drying. The dashed line is the reference without any rest between layers. W/C ratio is 0.2.

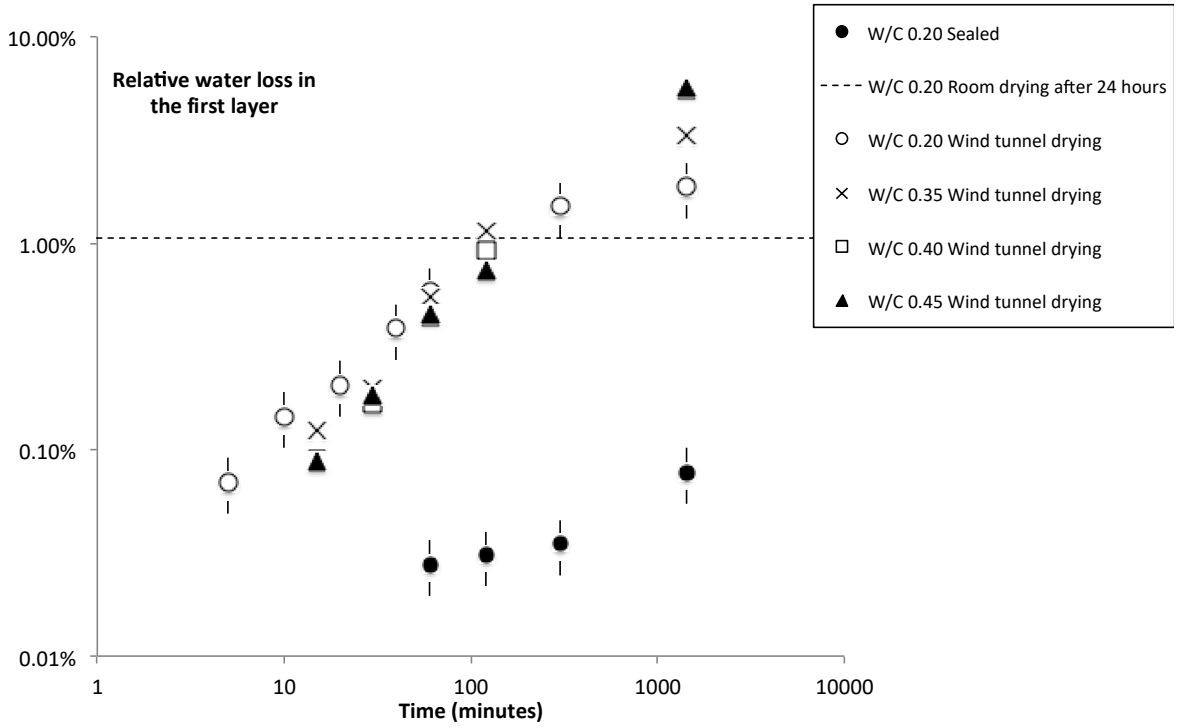

Figure 6. Relative water loss in the first layer (i.e. ratio between the amount of evaporated water and initial water content in the sample) as a function of resting time in wind tunnel, in laboratory room and sealed.

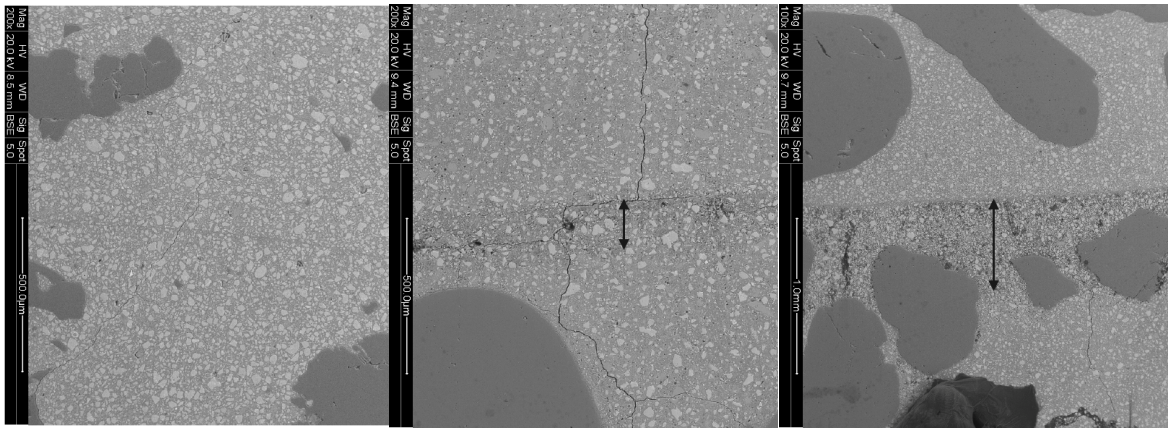

Figure 7. SEM pictures of the interface between layers. The first layer is at the bottom of each picture. (right) W/C ratio = 0.35 / 10 minutes resting time / sealed. (Center) W/C = 0.35 / 120 minutes resting time in wind tunnel. (Left) W/C = 0.35 / 24 hours resting time in wind tunnel.

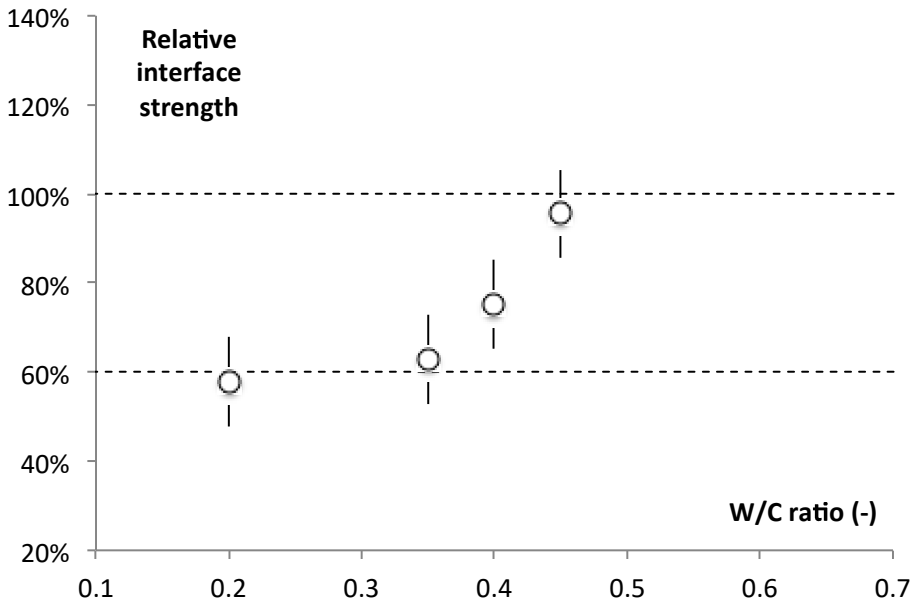

Figure 8. Relative interface strength as a function of W/C ratio after two hours rest between layers. Dashed lines represent respectively the reference level and the minimum value reached for W/C ratio lower than 0.35.

Table 1 Mix proportions and yield stresses of the mortars studied in this paper.

W/C	Sand volume fraction	HRWRA dosage (% of cement)	Yield stress
0.45	45%	No HRWRA	20 Pa
0.40	45%	Tempo 12, 0.40%	30 Pa
0.35	45%	Tempo 12, 0.75%	15 Pa
0.25	45%	Tempo 12, 2.50%	25 Pa
0.20	50%	Krono 947, 2.00%	35 Pa

TEST TYPE	NUMBER OF MEASUREMENTS	NUMBER OF SPECIMENS
BENDING TEST : REF	15	15
BENDING TEST : LAYERS	33	33
COMPRESSION TEST : REF	13	7
COMPRESSION TEST : LAYERS	23	12
BLADE TEST : REF	14	7
BLADE TEST : LAYERS	20	10
ANGLE TEST : REF	14	7
ANGLE TEST : LAYERS	22	11

Table 2. Number of measurements carried out in each configuration (Cf. Fig. 2) and used to assess the average and the standard deviation.